Supporting Information

Bimolecular Recombination Reactions: *K*-adiabatic and *K*-active Forms of RRKM Theory, Nonstatistical Aspects, Low Pressure Rates, and Time-Dependent Survival Probabilities with Application to Ozone. 2.

*Nima Ghaderi and R. A. Marcus**

Noyes Laboratory of Chemical Physics, California Institute of Technology, 1200 E. California Blvd., Pasadena, CA 91125, USA

S1. Method of Bimolecular Classical Trajectory with Action-Angle Variables

The initial conditions for the coordinates Q's and their conjugate momenta P's, for the atom-diatom system in action-angle variables, from the Appendix A from Part I,[S1] were either sampled in a canonical or a microcanonical regime, e.g. for k_{rec} and for $P(E,J,t)$. The equations of motion were then propagated, in the Jacobi internal coordinates for $O + O_2$ up until any reactive scattering and until the dissociation event.

A variant of LSODE[S2] (Livermore Solver for Ordinary Differential Equations), LSODA[S3] approach was used for switching between a non-stiff Adams method[S4] and a stiff Gear backward differentiation formula (BDF) method, a corrector-predictor algorithms,[S4] for propagating the equations of motion for the trajectories. LSODE and LSODA are library routines in ODEPACK.[S5] In LSODA, the data is dynamically monitored in order to decide which method to use in the next step. The algorithm also adaptively chooses both the order and the step size, where then subsequently a 2000 a.u. (48.38 fs) time bin size was selected for sampling the lifetime of O_3^* or the vdW complex from each individual trajectory for determining its $P(E,J,t)$.

As a check on the numerical stability of the algorithms and the proper performance of the simulation, the center-to-center distance R of O_3^* for some select trajectories were propagated backwards in time after the forward propagation of the equation of motion for R, by reversing the sign of the momenta, where the R reversed its direction as expected. The forward R minus the time reversed R for a select trajectory, i.e. its residual a_o (Bohrs), versus time varied by less than 0.001 % for a time of 10 ps.

Conservation of total energy as a function of time (ps) for select bimolecular trajectories for O_3^* was checked and the energy was conserved by 15 parts in 50000 for a

1000 ps lifetime trajectory, for an excess total energy $E = 0.2\ kT$ and $J = 15$. The magnitude of the total angular momentum J changed by 2 parts in 25000 for a given 1000 ps trajectory.

The number of trajectories used in the Figures and Tables in the text and in the Supporting Information are noted as follows:

Figures 1,2	2×10^4
Figure 3	5×10^3
Figure 4	3×10^3 for (a) and (c), 2×10^4 for (b)
Figure 5	5×10^3
Figure S1	5×10^4
Figure S2	4×10^3
Table 2	$(3 \text{ to } 5)\times10^3$
Table 4	$(2 \text{ to } 3)\times10^4$ for eq 10, various temperatures
Table S3	7×10^3 to 5×10^4 for eq 1, various temperatures

S2. The Potential Energy Surface for O_3

The ground state potential energy surface (PES) for O_3 used in the present study is based on that determined from Murrell and Varandas.[S6] In reference S6, an analytical function was constructed by combining spectroscopic data relating to the stable minima on the surface with quantum mechanical and kinetic data relating to other features of the surface. There, the surface was also parameterized to bring it into an approximate agreement with the *ab initio* results of Lucchese and Schaefer at the D_{3h} metastable minimum.[S6]

A parameter γ (not to be confused with the γ's in the text) that appears in both the coefficients of the interaction polynomial, eq 8, seen in Table 3 of ref S7 and in the long range term in eq 9 in ref S7, which appear in the PES in ref S6, was set to 4.36 in the present study in lieu of its initial value of 4.4. This modification ensured that any

isomerization of O_3^* during its complex lifetime remain less than a few percentage to match the results from experiment. As a check, the trajectory based k_{rec} was determined for the two values of γ noted above, and the k_{rec}'s agreed closely with each other.

The ground state frequency for the three normal modes of O_3, the bend, symmetric and antisymmetric mode were each calculated for this PES and each frequency was found to be within 2 %, 3 % and 2 %, respectively, of their experimental values.[S8] The equilibrium bond length, $r_e = 2.403$ a_o (Bohr) and the equilibrium apex angle $\alpha = 116.8^\circ$ for O_3 were each determined based on the PES and each found to be in agreement with their experimental values, $r_e = 2.415$ a_o, $\alpha = 116.8^\circ$. The dissociation energy, from the bottom of the potential well to the asymptote, for this PES is 1.13 eV which is smaller than the experimental value by 0.5 %.

S3. Identification of O_3^* and its Lifetime for the 1-TS and 2-TS Cases from Bimolecular Classical Trajectory

The lifetime of the ozone complex has been defined for both the 1-TS or the 2-TS case. For the case when k_{rec} from the bimolecular trajectory is determined for those intermediate complex that are confined to the inner transition state, then the complex lifetime is set to begin as soon as the reaction coordinate *R* crosses the inner TS, at about 5.2 a_o, the latter determined from variational RRKM theory, into the intermediate side, O_3^*. When no recrossing back is considered for this 1-TS case, the lifetime ends as soon as when *R* recrosses the inner TS out towards the reactant side $O + O_2$.

When recrossing is permitted, the reaction coordinate may cross or recross the inner and the outer TS for any multiple times, where the complex lifetime is initiated for these complexes in two ways: (1) R undergoes at least 3 turning points and the complex lifetime is terminated at the last turning point where R would then extend past a cutoff distance, set to 20 a_o so to confirm the event of dissociation, (2) as a check, a complex of O_3^* was declared when each bond of the complex underwent at least a full vibrational period where the lifetime was initiated at the first turning point of R and end at the last turning point of R. Both methods (1) and (2) were found to yield similar result for $P(E,J,t)$ and $W(E,J)$ of O_3^*.

For defining the lifetime of a vdW complex, the 3 turning point criterion of R was utilized. A vdW complex was identified according to when the newly formed incoming bond possessed the longest bond length, typically greater than 4 a_o, throughout the complex lifetime of the vdW intermediate. In contrast, O_3^* typically displayed an alternation of bond lengths throughout its lifetime. A vdW complex of O_3^* typically dissociated by 6ps. Unlike O_3^*, the intramolecular energy in the vdW complex is not expected to be shared optimally, since the longest bond typically remains at 4 a_o or greater. Although ~ 10 % vdW complexes formed out of the total trajectories at $E = 0.2$ kT and $J = 5$, and ~ 2 % vdW formed at $J = 15$, none of the vdW complexes adopted the geometric configuration of the usual O_3^* molecule.

S4. $\ln P(E,J,t)$ of O_3^* Versus Time

An additional select examples of the $\ln P(E,J,t)$ of O_3^* versus time (ps) for the entrance and exchange channels are shown in Figure S1. As discussed in the text, the offset of the entrance channel is shown to highlight the merge time of the survival probability, typically by 5 ps, as time elapses in the early times.

For the determination of $\ln P(E,J,t)$ vs time for the $J = 0$ case, Figure 3 in the main text, the initial conditions for the bimolecular trajectory entailed setting $m_j = -m_l$ since $M = 0,$ and the vectors $\vec{j} = -\vec{l}$.

(a)

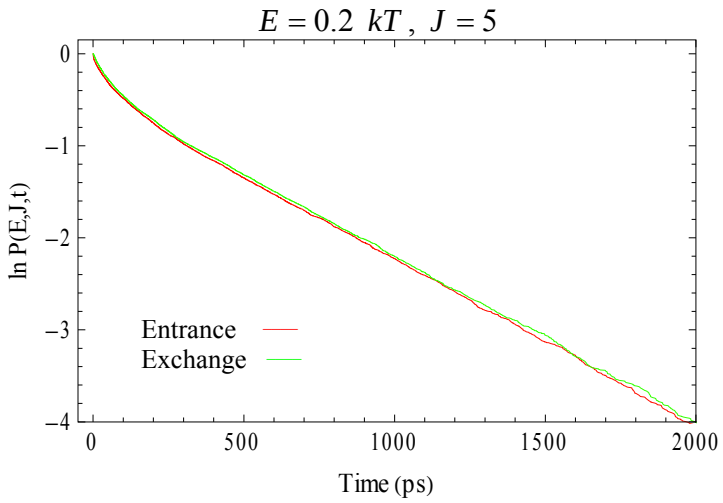

(b)

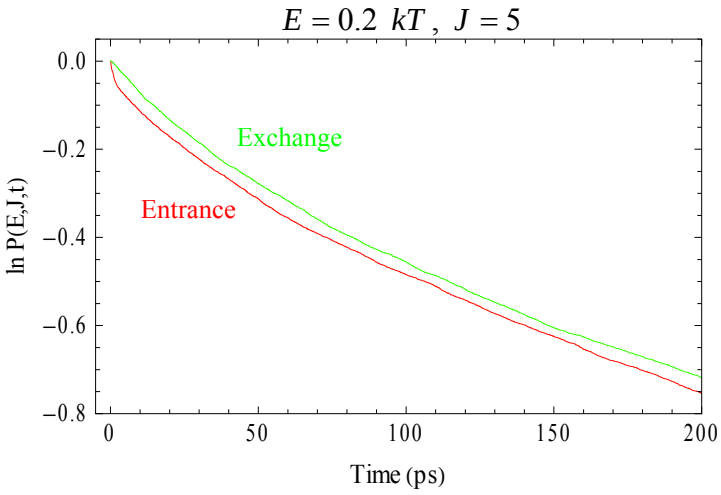

(c)

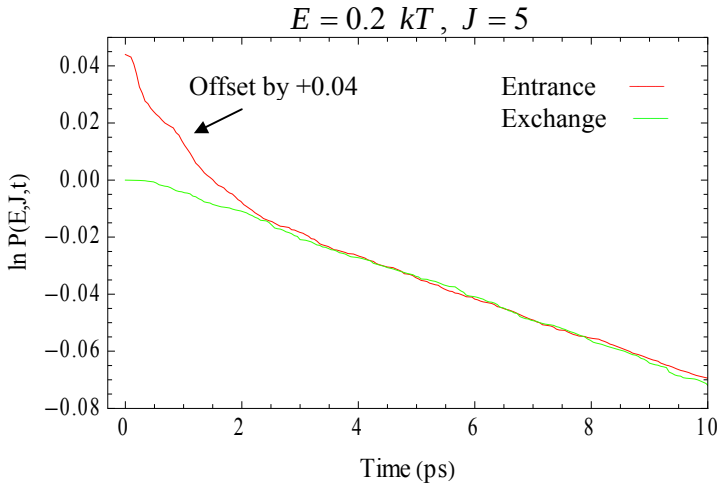

Figure S1. (a) The time-dependent survival probability, $\ln P(E,J,t)$ of O_3^* is plotted versus time (ps) for an excess total energy $E = 0.2\,kT$ and $J = 5$, using a bimolecular trajectory sampling. The entrance channel, the $\ln P_{en}(E,J,t)$ (——) and the exchange channel $\ln P_{ex}(E,J,t)$ (——). (b) Same as (a) but the first 200 ps zoomed, (c) the $\ln P_{en}(E,J,t)$ of the entrance channel is offsetted by +0.04 relative to $\ln P_{ex}(E,J,t)$ on the *y*-axis so to accentuate the drop-off in early times in the entrance channel. The time of the complete merging of both $P(E,J,t)$'s is seen to be about 3 ps.

S5. Histograms of ΔR for O_3^* at $J = 0$

Additional examples for a histogram of ΔR for O_3^* from the bimolecular trajectory, at $J = 0$ with $E = 0.2$, 0.5 and 1 *kT* are plotted in Figure S2. The plots indicate that as *E* increases from 0.2 to 1 *kT*, then the asymmetry in the ΔR at the earliest time decreases and becomes symmetric. The comparison of the $E = 0.2\,kT$, $J = 0$ plot in Figure S2a, with the $J = 15$ case (Figure 5) in the text, shows that for the $J = 0$ case an attenuation in the asymmetry of the ΔR is present during the early times for the O_3^*.

(a)

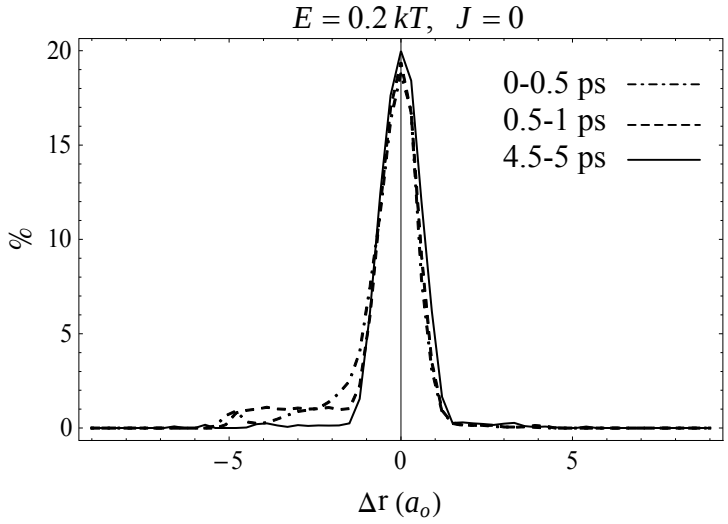
$E = 0.2\,kT,\ \ J = 0$
0-0.5 ps
0.5-1 ps
4.5-5 ps
%
Δr (a_o)

(b)

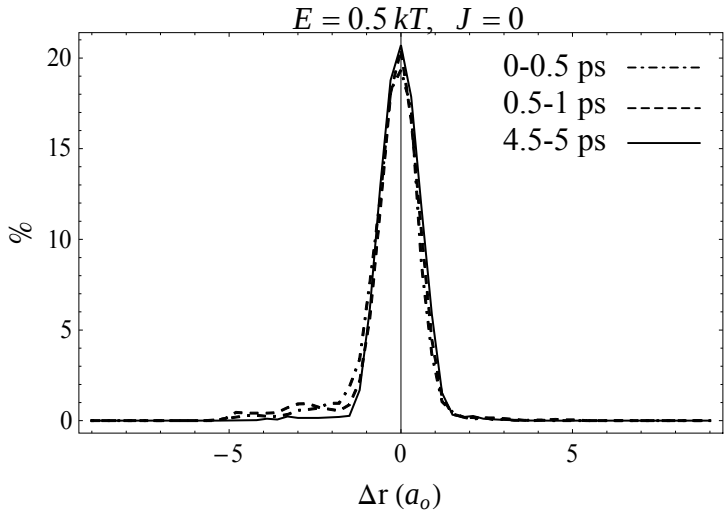
$E = 0.5\,kT,\ \ J = 0$
0-0.5 ps
0.5-1 ps
4.5-5 ps
%
Δr (a_o)

(c)

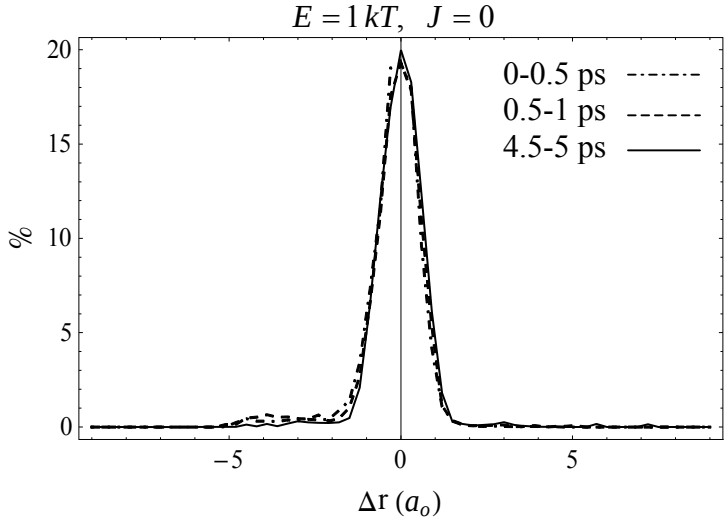
$E = 1\,kT,\ \ J = 0$
0-0.5 ps
0.5-1 ps
4.5-5 ps
%
Δr (a_o)

Figure S2. Histograms of Δr in Bohr radii for O_3^* formed from O + O_2 using classical trajectory for $J = 0$ and (a) $E = 0.2\ kT$, (b) $E = 0.5\,kT$, (c) $E = 1\,kT$. $\Delta r = r_1 - r_2$, where r_1 is the length of the existing bond, and r_2 is that of the newly formed bond for O_3^*. Shown for the time intervals: 0-0.5 ps (-···-), 0.5-1ps (----), 4.5-5 ps (—). The distribution is seen to become symmetric as time elapses and as *E* increases.

S6. The Initial Conditions for Trajectory Recrossings at the Transition State for O_3^* Using Action-Angle Variables

S6.1. Canonical Sampling at the TS

For sampling the initial conditions for the trajectory at the transition state, the total energy *E* and angular momentum *J* for O_3^* were selected using importance sampling. To eliminate redundancy, *J* was placed on the space fixed *z*-axis. The diatom angular momentum *j* was sampled in the range (0, $j_{\max}$), where $j_{\max} = (2EIkT)^{1/2}$ with *I* being the moment of inertia of the diatom. The orbital angular momentum *l* was determined from $l = j^2 + J^2 - 2jyJ$, where *y* was sampled from (-1,1) after transforming the variable m_j to *y*, where $y = m_j / j$. For a given *J* and m_j, then $m_l = J - m_j$, since $J = M$ where m_l also appears in the eqs A1-A12 of Part I for the *Q*'s and *P*'s. The internuclear distance *r* of the diatom was sampled between 2.2 and 3.0 a_o. The selection of this range for the limits of *r* was corroborated from the limits of *r* observed from the results of classical trajectories. Its conjugate momentum P_r was sampled from $(0, P_{r,\max})$, where $P_{r,\max} = (2E\mu_{bc})^{1/2}$. The w_j and w_l were sampled from a uniform distribution (0,1), while setting $(w_{m_j} = 0, w_{m_l} = 1/2)$.

Eqs A1-A3 and A7-A8 (Appendix A of Part I) for the Cartesian components for the coordinates *r* and *R*, respectively in terms of sampling their action-angle variables,

were determined and in turn used to determine the 3 internuclear distances of O_3^*, (R_1, R_2, R_3). The corresponding potential $V(R_1, R_2, R_3)$ was then determined. The conjugate momenta to *R*, the P_R was determined from the Hamiltonian, $H = j^2/2\mu_{bc}r^2 + l^2/2\mu_{abc}R^2 + P_r^2/2\mu_{bc} + P_R^2/2\mu_{abc} + V$. The Cartesian components of the conjugate momenta P1-P6 to the Q's, Appendix A of Part I, were also determined in terms of the action-angle variables. The value of *R* was set to the location of the inner transition state, about 5.2 a_o, where as noted earlier, the latter value was determined from variational RRKM theory. Both cases of the sign of P_R, either initially increasing or decreasing, were each sampled along with each of their time reversed dynamics for constructing the origin of each trajectory, for the purpose of determining the transmission coefficient.

S6.2. Microcanonical Sampling at the TS

The microcanonical sampling at the TS follows a similar procedure as for the canonical case in Section S6.1, except now the *E*'s and *J*'s are assigned their initial values, rather than importance sampled from their distribution.

S7. The Determination of the Transmission Coefficient κ for Forming O_3^* and Correcting $N^*(E,J)$ for Recrossings of the TS

The transmission coefficient,[S9] $\kappa = N_0/(N_0 + N_c)$ was determined for a select (E, J)'s and also for a thermal canonical distribution for various temperatures appearing as percentage of recrossings in Table 4 (column 4) in the text. The N_0 are those trajectories that lead directly to forming the product, in the present interest

identified as the metastable complex O_3^*, and N_c are the number of recrossings of *R* at the transition state.[S9] The representative set of trajectories from reactant to products, shown in Figure 1 of reference S9, were considered in the present analysis for any of their contribution to κ. The sampling of the initial conditions for each trajectory was performed at the TS where the flux in all directions were considered.

For determination of κ, only those trajectories with any of their recrossings, whose reaction coordinate *R* connected the reactant to product were considered in the determination of κ. Two necessary cases were considered, where each may contribute to κ and each were analyzed by identifying the set of trajectories that traverse from reactants $O + O_2$ to the metastable intermediate O_3^*: (1) the momentum P_R was initiated such that the value of *R* would decrease and the tally contributed to κ, only if the time reversed trajectory for the same initial conditions would have *R* either immediately or eventually, with any recrossings, return to the reactant state. These count as recrossings, since during the recrossing of the TS the *R* is no longer in the phase space of the ozone intermediate, but rather on the reactant side. Either the time reversed trajectory or the forward trajectory may have *R* of O_3^* recross the transition state an arbitrary number of times during its lifetime which was tallied in N_c. (2) The P_R was initiated such that the value of *R* would initially increase and checked to see if it ends on the O_3^* product side of the TS and also if its time reversed trajectory from the same initial conditions traced *R* back to the reactant $O + O_2$, with or without any recrossing of the TS, with *R* increasing beyond 20 a_o, then such tally contributed to κ. The results indicate that a negligible contribution is typically made to either N_c or N_0 in κ from case (2).

The *K*-active k_{rec} (RRKM) was corrected for recrossings of the transition state by multiplying the k_{rec} with the transmission coefficient e.g. $\kappa = 0.80$ at 298 K, reported in column 4 of Table 4, in the form of percentage of recrossings of the TS for various temperatures.

S8. The Determination of $N(E,J)$, $N^*(E,J)$, $W(E,J)$, and $\rho(E,J)$ for O_3

S8.1. $N(E,J)$ in Jacobi Action-Angle Variables

The treatment of $N(E,J)$ follows a similar description that followed eq 19 in Part I. Since either pair, ($w_{m_j} = 0, w_{m_l} = \pi$) or ($w_{m_j} = \pi$, $w_{m_l} = 0$), out of arbitrary pairs correspond to an identical ozone isomer, the first of the pair has been used. The total angular momentum *J* is placed on the space fixed *z*-axis. The j of the diatom was sampled between 0 and $j_{\max}$, where $j_{\max} = -2Ik_BT \ln E$, and *I*, the moment of inertia for the diatom was noted for each sampling of the variables in the integrand as the diatom internuclear distance *r* changed in the integrand.

The m_j was selected randomly in the range of ($-j$ to j). The w_j and w_l were each sampled from (0,1) where the angle γ between **r** and **R**, appearing in the potential explicitly depends on both w_j and w_l. The l was determined for each sampling point in the integrand from the j, m_j and *J* according to $l^2 = j^2 + J^2 - 2m_jJ$. The value of l is needed as it appears in the Hamiltonian, $H = j^2/2\mu_{bc}r^2 + l^2/2\mu_{abc}R^2 + p_r^2/2\mu_{bc} + P_R^2/2\mu_{abc} + V$. The P_R was integrated over and defined via the Hamiltonian. The p_r was sampled uniformly in the range from 0 (at

the asymptote) to the value given by the excess total energy above the asymptote and *r* was sampled from 2.2 to 3.0 a_o.

S8.2. $N^*(E,J)$ in Jacobi Action-Angle Variables

In obtaining $N^*(E,J)$, the variational RRKM theory was used to determine $N(E,J)$ as a function of *R*, where the minimum of the curve in the plots correspond to the minimum reactive flux which denotes the $N^*(E,J)$, as seen in Figure S2 for select values of *E* and *J*. Some typical values of $N^*(E,J)$ are given in Table 2 in the text. The non-random sampling methods and Monte Carlo methods with quasi and Adaptive approaches[S4] were each used to sample the variables in the integral with typically 1 million points and the results from each agreed to a few percentage with errors of 1 % in the final values.

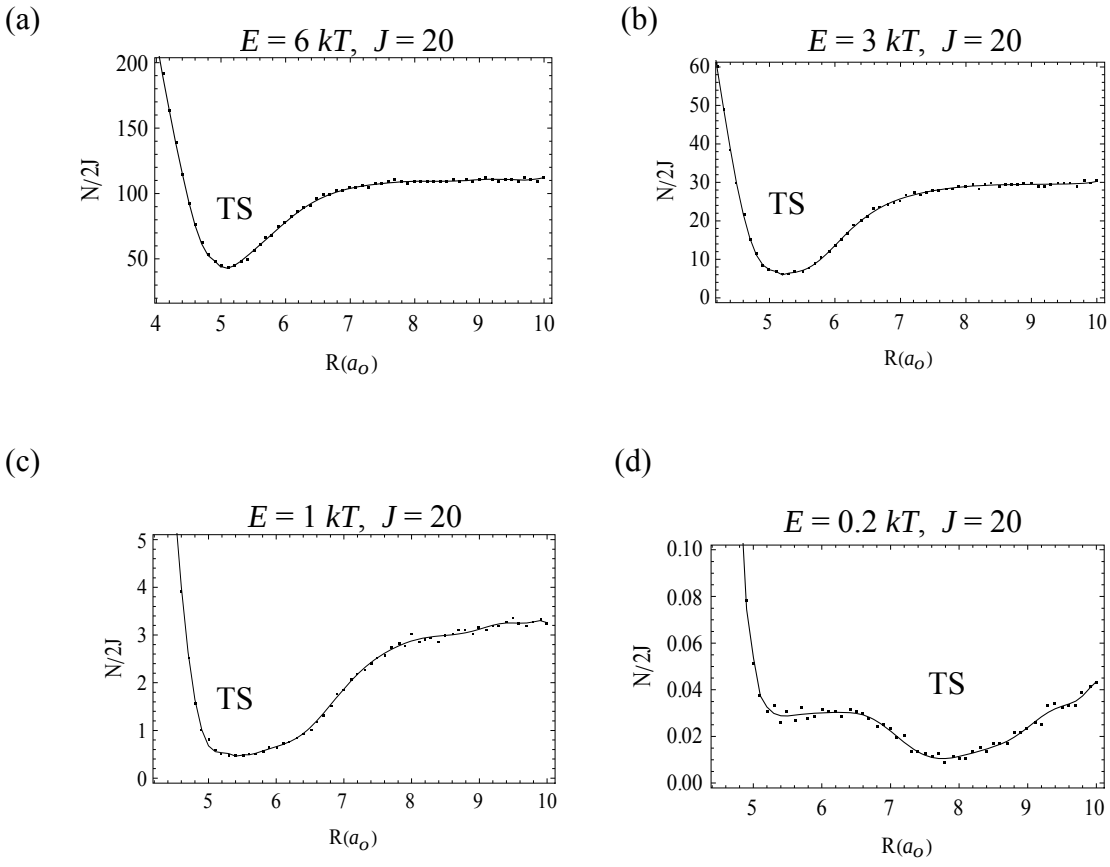

(e) (f)

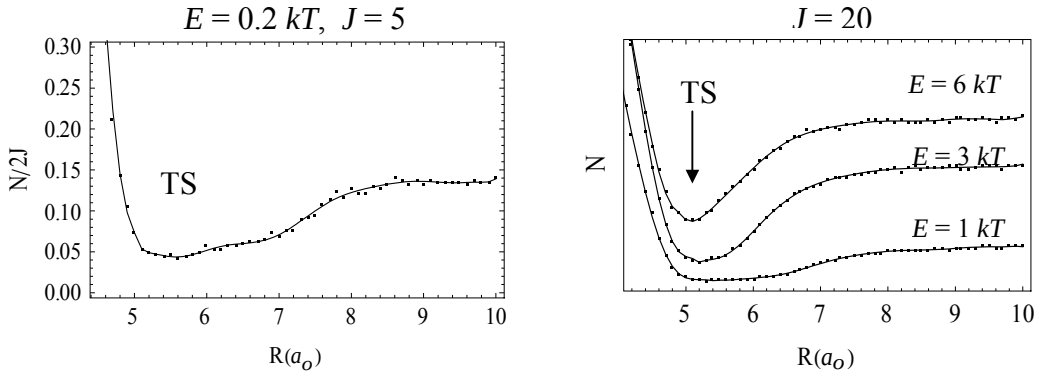

Figure S3. The number of states for O_3^* versus $R(a_o)$ are shown with their fits to a polynomial(—), using variational RRKM theory for various total excess energies $E(kT)$ and J's: (a) $E = 6\ kT$, $J = 20$, (b) $E = 3\ kT$, $J = 20$, (c) $E = 1\ kT$, $J = 20$, (d) $E = 0.2\ kT$, $J = 20$, (e) $E = 0.2\ kT$, $J = 5$, (f) $E = 1, 3, 6\ kT$, $J = 20$ superposed. The minima along R identifies the transition state (TS) as labeled.

S8.3. $W(E,J)$, Eq 4

For determining $W(E,J)$, eq 4, the vibrational n was selected to lie in $(0,\ n_{\max})$, with $n_{\max} = E/h\nu$ and j selected to lie in $(0, j_{\max})$, with $j_{\max} = \sqrt{2I/\hbar^2(E - nh\nu)}$, where I is the moment of inertia of the diatom and ν is the fundamental vibrational frequency of the diatom, under the additional constraint of $E_{vib} + E_{rot} \le E$ to ensure conservation of total energy. It is useful to restrict j in this way, to reduce the sample space, since it not only restricts j but also serves to restrict l via $l^2 = j^2 + J^2 - 2m_j J$. The Jacobian of a transformation is then introduced for changing l to m_j. The integration limits for m_j are $(-j, j)$, with a Jacobian of $1/(dl/dm_j)$ equal to $J/(j^2 + J^2 - 2m_j J)^{1/2}$. The integration variable m_j was transformed to y where $y = m_j / j$, with a Jacobian of j. The latter transformation permits a fixed lower and

upper integration limits (-1,1) for *y*, instead of the limits for m_j, for a changing j. As a check, using either the limits for *y* or for m_j yielded the same answer.

Select values for $W_{ex}(E,J)/W_{en}(E,J)$ and $W_{ex}(E,J)P(E,J)_{ex}/W_{en}(E,J)P(E,J)_{en}$ for O_3^*, in addition to those given in the text, are given in Tables S1 and S2, respectively:

Table S1: The ratio W_{ex}/W_{en} for select values of *E* (*kT*) and *J* for O_3^*.

	E	W_{ex}/W_{en}		*E*	W_{ex}/W_{en}
$J=1$	1	0.99	$J=5$	1	0.98
	0.5	0.98		0.5	0.89
	0.2	0.94		0.2	0.85
	0.1	0.92		0.1	0.89
$J=10$	1	0.92	$J=15$	1	0.89
	0.5	0.87		0.5	0.87
	0.2	0.85		0.2	0.86
	0.1	1.00		0.1	0.91
$J=20$	1	0.89	$J=25$	1	0.85
	0.5	0.85		0.5	0.86
	0.2	1.00			

Table S2: The ratio $W_{ex}(E,J)P(E,J)_{ex}/W_{en}(E,J)P(E,J)_{en}$ for select values of E (kT) and J for O_3^*.

	E	$W_{ex}P_{ex}/W_{en}P_{en}$		E	$W_{ex}P_{ex}/W_{en}P_{en}$
$J=1$	1	1.03	$J=5$	1	0.80
	0.5	0.95		0.5	0.81
	0.2	0.94		0.2	0.82
	0.1	0.90		0.1	0.86
$J=10$	1	1.00	$J=15$	1	1.00
	0.5	0.85		0.5	0.87
	0.2	0.91		0.2	0.85
	0.1	0.94		0.1	0.91
$J=20$	1	1.08	$J=25$	1	0.95
	0.5	0.90		0.5	0.73
	0.2	0.90			

S8.4. $\rho(E,J)$ in Normal Mode Coordinates with Harmonic Approximation

As an approximate check on the calculation of $\rho(E,J)$, the latter is also determined in the harmonic approximation.[S10] In the harmonic approximation,

$$\rho(E,J)=\frac{2J}{2!\prod_{j=1}^{s}v_j}\int\Theta[E-H'(K)]dK\,, \tag{S1}$$

where $H'=J^2/2I_2+(1/2I_1-1/2I_2)K^2$, I_1 and I_2 are the principal moments of inertia, with the prolate approximation $I_1<I_2\approx I_3$ for O_3, the K is the projection of J on the principal axis I_1 spanning the range $-J\le K\le J$, $s=3$ is the number of oscillators, v_i is the i'th harmonic frequency (bend, symmetric and antisymmetric modes obtained from the present potential), and Θ is the unit step function. The $2J$ accounts for the degeneracy of M, the projection of J on the z-axis of the space fixed coordinate. In this prolate symmetric top approximation for $\rho(E,J)$, the rotation-vibrational coupling and

the anharmonicity of the O_3 potential are omitted. The ratios of the exact $\rho(E,J)$ with the actual potential using Euler angular momenta with normal coordinates, eq 14, to the harmonic based $\rho(E,J)$, eq S1, as a function of (E,J) were determined. Typically, the ratio of the exact to the harmonic treatment of $\rho(E,J)$ was found to be ~ 1.5 for the (E,J) region of interest, a result found in an earlier study.[S11]

S9. Weak Collision Parameters for $Z(E',E)$

At sufficiently low pressures, each $O_3^*(E')$, formed from a bimolecular reaction, $M + O_3(E) \underset{Z(E,E')}{\overset{Z(E',E)}{\rightleftarrows}} M + O_3^*(E')$ with $E' \geq 0$, ultimately dissociates into O + O_2 before any further collision with a third body *M*. Sampling from a unimolecular process may not lead to dissociation due to quasi-periodic trajectories. The $Z(E',E)$ that appears in the expressions for k_{rec} is approximated to be the product of a collision number, Z_o, and the normalized probability of energy transferred per collision per unit energy $P(E',E)$, considered here for a single exponential model for the deactivation process of the intermediate,[S12-S14] $\exp[-(E-E')/\gamma]/(\gamma+\gamma')$ with $E \geq E'$, where γ is the average deactivation energy transferred from the intermediate to a bath gas molecule in a deactivating collision. In turn, γ is related to the average energy transferred for an activating collision γ' by microscopic reversibility. In the present calculations, γ has been set to 85.5 cm^{-1},[S15] noted as 85 cm^{-1} in the text, approximately 0.41 *kT*, at $T = 298$ K. While it has a significant uncertainty, since it rests on several assumptions[S15] including a weak temperature of the average internal energy transfer per collision,

whereas collisional calculations using Argon as a bath gas showed a marked temperature dependence.[S16]

For Z_o, it may be assumed that a deactivating collision between a vibrationally excited ozone molecule and a bath gas molecule is governed by a Lennard-Jones type potential,[S17] $V_{LJ} = 4\varepsilon\left[\left(\frac{\sigma}{r}\right)^{12} - \left(\frac{\sigma}{r}\right)^{6}\right]$, where σ and ε are the standard interaction parameters for which we have assumed literature values, $\sigma = 3.889$ Å for N_2 and $\varepsilon = 107.3$ K.[S18] The Lennard-Jones collision number is given by[S19] $Z_{LJ} = 8.09\times10^{-10}\sqrt{\frac{T}{1000}}\sqrt{\frac{20}{\mu_{O_3,N_2}}}\left(\frac{\sigma}{5}\right)^2\Omega^*_{2,2}$ cm^3 molecule^{-1} s^{-1}. The quantity μ_{O_3,N_2} is the reduced mass of the ozone-nitrogen pair in amu, T is the absolute temperature, and the collision integral $\Omega^*_{2,2}$ is approximately given by[S19,S20] $\Omega^*_{2,2} = 1.16145(T^*)^{-0.14874} + 0.52487e^{-0.7732T^*} + 2.16178e^{-2.437887T^*}$, where T^* is the reduced temperature, $T^* = \frac{T}{\varepsilon}$. At $T = 298$ K and utilizing the values for the aforementioned parameters yields $Z_{LJ} = 3.01\times10^{-10}$ cm^3 molecule^{-1} s^{-1} for O_3.

S10. Bimolecular RRKM k_{rec} for O_3

S10.1. *K*-active

The *K*-active $k_{rec}(RRKM)$, eq 13, O_3 was determined from an ensemble of samplings in (E,J) space using the distribution in the integrand. As a check, the density of states $\rho(E,J)$ was first determined as a function of (E,J), and this sampling function for $\rho(E,J)$ was then utilized in eq 13 and sampled along with the remaining integrand

over the variables *E* and *J*, which proceeded efficiently with a quadrature method where the results agreed with the first method. Adaptive algorithms for integrating eq 13 yielded similar results for $k_{rec}(RRKM)$. The function $\Theta(E,J)$ was determined separately for when the flux at the TS towards forming O_3^* is nonzero and taken into consideration in the integrand for each set of sampling points in the integrand. As an additional check on $k_{rec}(RRKM)$, eq 13 was determined for $k_{rec}(RRKM)$ at (E,J)'s of interest. These $k_{rec}(E,J)$'s were then summed over the (E,J) space to yield the final $k_{rec}(RRKM)$. This entailed acquiring the $\rho(E,J)$ and $\Theta(E,J)$ separately for each (E,J) resolved integrand in eq 13. The final result for $k_{rec}(RRKM)$ from the latter method agreed with the other aforementioned methods.

S10.2. *K*-adiabatic

The *K*-adiabatic $k_{rec}(RRKM)$, eq 17, for O_3 was determined (1) in a similar way as eq 13, the latter noted in Section S10.1, but the $\Theta(E,J,K)$ and $\rho(E,J,K)$ were instead utilized, rather than $\Theta(E,J)$ and $\rho(E,J)$. Ensemble of sampling of the Euler angular momenta with normal coordinates for O_3 were selected in eq 17, and also using eq 18 for the $\rho(E,J,K)$. The $\Theta(E,J,K)$ was determined separately from variational RRKM theory, and then used in the integrand. The value of *K*'s greater than ~5 made negligible contribution to the integrand, yielding the value 5.4×10^{-34} cm^6 molecule^{-2} s^{-1} for the *K*-adiabatic $k_{rec}(RRKM)$. The determination of $k_{rec}(RRKM)$ for the various temperatures in Table 4 entailed evaluating the partition functions for the select temperature, and all other quantities with a functional dependence of *T* in the expression.

S11. Bimolecular Trajectory k_{rec} for O_3

The bimolecular trajectory based k_{rec} was determined in (1) the total J representation in Jacobi coordinates with action-angle variables, using eq 10 and, (2) k_{rec} was also determined in an equivalent representation $(dldm_l djdm_j dndw_l dw_{m_l} dw_j dw_{m_j} dw_n)$, eq 1. The k_{rec}'s for various temperatures, for each channel, for the above methods are reported in Table S3, where these values are reported to agree to within a few percent of each other.

For the above methods (1) and (2), the thermal survival probability was determined separately and then placed in the recombination integral and integrated over in time. As another check, the survival probability for O_3^* was also constructed in real time as the sampling of the trajectories proceeded and its sampling also performed in real time as well, and its contribution to the integrand was tallied for a given intermediate from its trajectory, which yielded results to within a few percent. The convergence of the final answer was verified to a few percent. The computations for k_{rec} were repeated and the results were also reproduced.

Table S3. Comparison of the bimolecular trajectory k_{rec} ($\times 10^{-34}$) for O_3 based on eqs 1 and 10 as defined in the text.[a]

Temperature (K)	eq 1			eq 10		
	ex	*en*	*en/ex*	*ex*	*en*	*en/ex*
130	55.2	59.4	1.08	54.0	59.2	1.10
200	10.9	11.9	1.09	10.7	11.7	1.09
298	2.24	2.53	1.13	2.26	2.56	1.13
373	0.85	0.98	1.15	0.86	0.97	1.13

[a] The k_{rec}'s are reported for a reaction with distinguishable atoms, A+BC→AB+C, single isomer of O_3, ABC in the low pressure region $(Z = 0)$. Unit of k_{rec} is cm^6 $molecule^{-2}$ s^{-1}.

S12. Bimolecular Trajectory k_{rec} for O_3 from vdW Complex

In addition to the complex of O_3^* that forms from O + O_2, a van der Waals (vdW) complex $O_2 \cdots O$ may also form where the incoming bond typically stays the longest during its lifetime. Like the usual O_3^*, at any given *E*, as *J* increases then the number of vdW complex decreases, and as *E* increases then the formation of vdW also further decreases. Typically 10 % of the reactive collision complexes from O + O_2 yielded a vdW complex and 30 % gave rise to the O_3^* complex for a given energy, where these percentages decreased as *J* increased for either type of complex.

In the bimolecular classical trajectory study at a given (*E,J*), those complexes that form a vdW complex from an O + O_2 were identified, and their time dependent survival probability and $W(E,J)$'s were determined and then used to obtain its k_{rec}. The (E,J) resolved recombination rate constant for forming O_3, using eq 10 in the text, from a vdW complex was determined for different (E,J)'s. The integration over the initial conditions, at $T = 298\,\mathrm{K}$ and low pressure $(Z = 0)$, yields 6.6×10^{-41} cm^6 molecule^{-2} s^{-1} for the k_{rec} of a given isomer of O_3 from a vdW complex, where vdW was initially formed from O + O_2. The k_{rec} from vdW is seen to be negligible relative to the k_{rec} of O_3, 4.8×10^{-34} cm^6 molecule^{-2} s^{-1}, considered for a given isomer of O_3 at 298 K, and also negligible at other temperatures.

The contributions to the k_{rec} of O_3 from the vdW is as follows: for a vdW complex the collisional stabilization cross section, $\sigma_{stab} = 5.0\times10^{-2}\,a_0^2$ from a wavepacket study that used Ar as a bath gas molecule,[S21] is about 100 times smaller than for the usual

complex. In turn, the σ_{stab} yields a stabilizing collision frequency k_{stab} for the vdW complex, 8.0×10^{-14}, which is smaller than for the usual complex by about a factor of 2700, ($k_{stab} = \Omega_{2,2}\sigma_{stab}\upsilon$, and $\Omega_{2,2}$ is the collision integral and υ is the velocity of the colliders). The $P(E,J,t)$ and $W(E,J)$ for vdW further reduce its k_{rec}. For the entrance channel the $P(E,J,t)$'s for the vdW complex at most survive up to 6 ps at the lower energies, and the survival times decrease as *E* and *J* increases. These shorter $P(E,J,t)$'s for the vdW complex also contribute less to the k_{rec} relative to the usual O_3, whose lifetime may be longer than 200 ps at the lower energies.

References

(S1) Ghaderi, N.; Marcus, R.A. Bimolecular Recombination Reactions: Low Pressure Rates in Terms of Time-Dependent Survival Probabilities, Total *J* Phase Space Sampling of Trajectories, and Comparison with RRKM Theory. *J. Phys. Chem.* B. **2011**, *115*, 5625-5633, denoted as Part I.

(S2) Hindmarsh, A.C. LSODE and LSODI, Two New Initial Value Ordinary Differential Equation Solvers. *ACM SIGNUM Newsletter* **1980**, *15*, No. 4, 10-11.

(S3) Petzold, L. Automatic Selection of Methods for Solving Stiff and Nonstiff Systems of Ordinary Differential Equations. *SIAM J. Sci. Stat. Comput.* **1983**, *4*, 136-148.

(S4) Press, W.H.; Flannery, B.P.; Teukolsky, S.A.; Vetterling, W.T. *Numerical Recipes: The Art of Scientific Computing*; Cambridge University Press: New York, **2007**.

(S5) Hindmarsh, A.C. "ODEPACK, a Systematized Collection of ODE Solvers", *Scientific Computing*, edited by R.S. Stepleman *et al*.; North-Holland, Amsterdam, **1983**, p. 55.

(S6) Varandas, A.J.C.; Murrell, J.N. Dynamics of the $^{18}O + {}^{16}O_2$ (υ=0) Exchange Reaction on a New Potential Energy Surface for Ground-state Ozone. *Chem. Phys. Lett.* **1982**, *88*, 1-6.

(S7) Murrell, J.N.; Sorbie, K.S.; Varandas, A.J.C. Analytical Potentials for Triatomic Molecules from Spectroscopic Data II. Application to Ozone. *Molec. Phys.* **1976**, *32*, 1359-1372.

(S8) Barbe, A.; Secroun, C.; Jouve, P. Infrared Spectra of $^{16}O_3$ and $^{18}O_3$: Darling and Dennison Resonance and Anharmonic Potential Function of Ozone. *J. Molec. Spect.* **1974**, *49*, 171-182.

(S9) Anderson, J.B. Statistical Theories of Chemical Reactions. Distributions in the Transition Region. *J. Chem. Phys.* **1973**, *58*, 4684-4692.

(S10) Marcus, R.A. Unimolecular Dissociations and Free Radical Recombination Reactions. *J. Chem. Phys.* **1952**, *20*, 359-364.

(S11) Gao, Y.Q.; Marcus, R.A. On the Theory of the Strange and Unconventional Isotopic Effects in Ozone Formation. *J. Chem. Phys.* **2002**, *116*, 137-154.

(S12) Tardy, D.C.; Rabinovitch, B.S. Collisional Energy Transfer. Thermal Unimolecular Systems in the Low-Pressure Region. *J. Chem. Phys.* **1966**, *45*, 3720-3730.

(S13) Troe, J. Theory of Thermal Unimolecular Reactions at Low Pressures. I. Solutions of the Master Equation. *J. Chem. Phys.* **1977**, *66*, 4745-4757.

(S14) Zhu, Z.; Marcus, R.A. On Collisional Energy Transfer in Recombination and Dissociation Reactions: A Wiener-Hopf Problem and the Effect of a Near Elastic Peak. *J. Chem. Phys*. **2008**, *129*, 214106/1-10.

(S15) Hippler, H.; Rhan, R.; Troe, J. Temperature and Pressure Dependence of Ozone Formation Rates in the Range 1-1000 bar and 90-370 K. *J. Chem. Phys.* **1990**, *93*, 6560-6569.

(S16) Ivanov, M.V.; Schinke, R. Temperature Dependent Energy Transfer in Ar-O_3 Collisions. *J. Chem. Phys.* **2005**, *122*, 234318/1-6.

(S17) Hill, T.L. *An Introduction to Statistical Thermodynamics*; Dover: New York, **1986**, and references cited therein.

(S18) Kaye, J.A. Theoretical Analysis of Isotope Effects on Ozone Formation in Oxygen Photochemistry. *J. Geophys. Res.* **1986**, *91*, 7865-7874.

(S19) Smith, S.C.; Gilbert, R.G. *Theory of Unimolecular and Recombination Reactions*; Blackwell Scientific Publications: Oxford, UK., **1990**, and references cited therein.

(S20) Reid, R.C.; Prausnitz, J.M.; Sherwood, T.K. *The Properties of Gases and Liquids*, 3rd ed. McGraw-Hill: New York, **1977**.

(S21) Ivanov, M.V.; Babikov, D. Collisional Stabilization of van der Waals States of Ozone. *J. Chem. Phys.* **2011**, *134*, 174308/1-11.